On the nature of homo- and hetero-dinuclear metal–metal quadruple bonds — Analysis of the bonding situation and benchmarking DFT against wave function methods

Nozomi Takagi, Andreas Krapp, and Gernot Frenking

Abstract: Homo- and hetero-dimetallic $(d–d)^8$ analogues of the formally quadruply bonded $[Re_2Cl_8]^{2–}$ system with the general formula $[MM'Cl_8]^x$ (M, M′ = Tc, Re, Ru, Os, Rh, Ir and x = –2, –1, 0, +1, +2) have been calculated with the density functional theory (DFT) functionals SVWN, BLYP, BP86, PBE, OLYP, OPBE, HCTH, B3LYP, O3LYP, X3LYP, BH&HLYP, TPSS, VSXC, TPPSh, and ab initio methods (CASPT2, CCSD(T)) using basis sets of triple-ζ quality. The performance of the functionals for the description of the metal–metal bond distance and the bond dissociation energy as well as the singlet–triplet gap was evaluated with respect to ab initio data at the CASPT2 level. Generally, the generalized gradient approximation (GGA) functionals, BLYP, BP86, and PBE, show good performance in the description of the metal–metal bond distance and for the dissociation energy. Hybrid functionals are not to be used for compounds of the type discussed here as they lead to increasingly too short and too weak bonds with the amount of exact exchange included. All functionals underestimate the singlet–triplet gap, with the GGA functionals BLYP, BP86, PBE being the closest to the CASPT2 values. The bonding situations of the $[MM'Cl_8]^x$ compounds were analyzed at the DFT level (BP86) using the natural bond orbital (NBO) method and the energy decomposition analysis. The M–M bond in homodimetallic compounds, $[MMCl_8]^x$, becomes weaker from group 7 to group 8 to group 9 metals and the bond is weaker for 4d metal systems than for 5d transition metal compounds. The M–M bonds have approximately 50% covalent and 50% electrostatic character and the covalent contribution is dominated by the π orbitals, whereas the δ orbitals do not contribute significantly to the covalent bonding. Heterodimetallic systems, $[MM'Cl_8]^x$, have significantly stronger metal–metal bonds than the homodimetallic compounds. This comes from weaker Pauli repulsion and stronger electrostatic attraction. The most stable heterodimetallic bonds are observed for 5d–5d metal pairs.

Key words: metal–metal bond, metal–metal quadruple bond, heterodimetallic compounds, homodimetallic compounds, dissociation energy, bonding analysis.

Résumé : On a effectué des calculs théoriques sur des analogues homo- et hétéro-dimétalliques $(d–d)^8$ du système $[Re_2Cl_8]^{2–}$ formellement à quadruple liaison et de formule générale $[MM'Cl_8]^x$ (M, M′ = Tc, Re, Ru, Os, Rh et Ir et x = –2, –1, 0, 1 et +2) en faisant appel à la théorie de la fonctionnelle de la densité (« DFT »), des fonctionnelles SVWN, BLYP, BP86, PBE, OLYP, OPBE, HCTH, B3LYP, O3LYL, BH&HLYP, TPSS, VSXC, TPPSh et des méthodes ab initio [CASPT2 et CCSD(T)] à base d'ensembles de qualité triple ζ. On a évalué la performance des fonctionnelles pour la description de la longueur de la liaison métal-métal et de l'énergie de dissociation de la liaison ainsi que l'intervalle singulet-triplet par rapport aux données ab initio au niveau CASPT2. En général, les fonctionnelles GGA BLYP, BP86 et PBE donnent une bonne performance dans la description de la longueur de la liaison métal-métal et pour l'énergie de dissociation. Il ne faut pas utiliser les fonctionnelles hybrides pour le type de composés discutés ici parce qu'elles conduisent à des longueurs de liaison qui sont de plus en plus trop courtes et des énergies de liaison trop faibles pour les quantités exactes d'échange incluses. Toutes les fonctionnelles sous estiment l'intervalle singulet-triplet avec les fonctionnelles GGA BLYP, BP86 et PBE conduisant aux valeurs les plus près de valeurs CASPT2. On a examiné les situations de liaison des composés $[MM'Cl_8]^x$ à l'aide de la « DFT » au niveau BP86, en utilisant la méthode NBO et l'analyse de la décomposition de l'énergie. La liaison M–M des composés homodimétalliques $[MMCl_8]^x$ devient de plus en plus faible lorsqu'on passe des éléments du groupe 7, à ceux des groupes 8 et 9 et la liaison est plus faible pour les systèmes métalliques 4d que pour les composés métalliques de transition 5d. Les liaisons M–M comportent des quantités approximativement égales 50/50, de caractère covalent et électrostatique; la contribution covalente est dominée par les orbitales π alors que les orbi-

Received 18 February 2010. Accepted 5 May 2010. Published on the NRC Research Press Web site at canjchem.nrc.ca on 10 September 2010.

This article is part of a Special Issue dedicated to Professor R. J. Boyd.

N. Takagi and G. Frenking.[1] Fachbereich Chemie, Philipps-Universität, Hans-Meerwein-Strasse, D-35039 Marburg, Germany.
A. Krapp. Fachbereich Chemie, Philipps-Universität, Hans-Meerwein-Strasse, D-35039 Marburg, Germany; Senter for teoretisk og beregningsorientert kjemi, Kjemisk institutt, Universitetet i Oslo, Postboks 1033 Blindern, 0315 Oslo, Norway.

[1]Corresponding author (e-mail: frenking@chemie.uni-marburg.de).

tales δ ne contribuent pas d'une façon significative à la liaison covalente. Les systèmes hétérodimétalliques $[MM'Cl_8]^x$ comportent des liaisons métal-métal qui sont beaucoup plus fortes que celles des composés homodimétalliques. Cette situation résulte de la répulsion de Pauli et d'une attraction électrostatique plus forte. Les liaisons hétérodimétalliques les plus stables sont observées pour les paires métalliques 5d–5d.

Mots-clés : liaison métal–métal, liaison quadruple métal–métal, composés hétérodimétalliques, composés homodimétalliques, énergie de dissociation, analyse des liaisons.

[Traduit par la Rédaction]

Introduction

The exploration of the chemistry of metal–metal multiple bonds started in 1965 when Cotton and Harris[1] isolated the anion $[Re_2Cl_8]^{2-}$ in the complex $K_2[Re_2Cl_8]\cdot 2H_2O$. This compound with a formal Re–Re quadruple bond has since become the prototype of a metal–metal multiple bonded species. Its electronic structure is known in detail and a gas-phase photoelectron spectrum has been collected.[2] Following this initial discovery, the field expanded considerably and a wealth of knowledge has been gained as reflected in the prominent book by Cotton, Murillo, and Walton,[3] which covers the literature up to 2004. In recent years, the field came into general focus again, as exemplified by the isolation of the formally quintuply bonded compound RCr–CrR (R = C_6H_3-2,6(-C_6H_3-2,6-*i*-$Pr_3)_2$) by the group of Power[4] and by a number of recent quantum chemical studies about molecules with high bond orders between metal atoms.[5–7]

In the last 20 years, heterodinuclear compounds between different metal atoms M–M′ were studied experimentally due to their potential as catalysts in metal-mediated reactions, as exemplified by the "early–late" complexes, which mainly contain metal–metal single bonds.[8–11] Much less is known about polar metal–metal bonds of higher bond multiplicity.[3,12] Collmann and Boulatov[12] reported in a series of studies about the structures and intriguing spectral properties of systems with polar metal–metal multiple bonds with the general formula PorM–M′Por (Por = substituted porphyrins).

Little is known about the bonding situation and the stability of these polar metal–metal multiple bonds from a theoretical point of view. As a first step towards the description of the experimentally known systems and the systematic exploration of the bonding possibilities in polar metal–metal multiple bonding, we set out a systematic study of heterodimetallic analogues of $[Re_2Cl_8]^{2-}$. The results of the work are reported in this paper. We focused on the formally quadruply bonded (d–d)[8] systems with the general formula $[Cl_4MM'Cl_4]^x$ (M, M′ = Tc, Re, Ru, Os, Rh, Ir; x = –2, –1, 0, +1, +2). We did not include the analogues of the first row transition metals (Mn, Fe, Co) in our study, since explorative calculations on the systems $[M_2Cl_8]^x$ showed that they are unbound and because of the highly multideterminental character inherent in these species, demand far too large active spaces to be tractable. Since our intention was to shed light onto the metal–metal quadruple bond, we restricted ourselves to geometrical arrangements, which enable two MCl_4^x fragments to form a metal–metal quadruple bond. This is the D_{4h} (C_{4v} for heterodimetallic systems) symmetric structure (see Scheme 1), which might not be the global minimum for all species studied.

Metal–metal bonded systems are typical examples of multideterminant problems. We therefore tested the performance of a variety of density functional theory (DFT) functionals in comparison to theoretical results at the CASPT2 and CCSD(T) levels of theory. The bonding situation of the formally metal–metal bonded systems was studied in detail, making use of the energy decomposition analysis (EDA) and the natural bond orbital method (NBO).

Scheme 1.

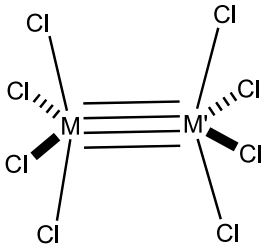

Computational methods

For benchmarking the performance of DFT we tested the following functionals: (*i*) local density approximation (LDA): SVWN;[13,14] (*ii*) generalized gradient approximation (GGA): BP86,[15,16] BLYP,[15,17] OLYP,[17,18] OPBE,[18,19] PBE (also called PBEPBE),[19] and HCTH (also called HCTH407);[20] (*iii*) hybrid GGA: B3LYP,[15,17,21] BH&HLYP,[15,17,22] O3LYP,[15,17,23] and X3LYP;[17,24] (*iv*) meta-GGA: TPSS (also called TPSSTPSS)[25] and VSXC;[26] and (*v*) hybrid meta-GGA: TPSSh.[25]

We used split-valence basis sets of doubly polarized triple-ζ quality developed by Weigend[27] and Ahlrichs,[28] which are denoted as def2-TZVPP. For the metal atoms we used valence basis sets in conjunction with small-core quasi-relativistic effective core potentials.[29] The DFT calculations were performed with the Gaussian03 program package[22] using standard settings for the DFT integration (fine grids) and for the convergence criteria. Care has been taken to obtain the correct electronic states, e.g., $^1A_{1g}$ states for the D_{4h} symmetry $[M_2Cl_8]^x$ molecules and $^1A_1$ states for the C_{4v} symmetric $[MM'Cl_8]^x$ systems.

Single point energy calculations using coupled cluster theory[30] at the CCSD(T) level[31–35] in conjunction with the def2-TZVPP basis set were performed on BP86/TZ2P geometries (the TZ2P basis set will be specified below) with the program MolPro2006.[36] To account for static and dynamic correlation effects by wave function methodology, we performed complete active space (CAS) SCF[37] calculations with the dynamic correlation added by multiconfigurational second-order perturbation theory (CASPT2).[38–40] Scalar relativistic effects were included via a Douglas–Kroll Hamiltonian.[41,42] Large ANO-RCC basis sets of Roos and

Table 1. Optimized metal–metal distances in Å of $[MM'Cl_8]^x$ in the lowest totally symmetric closed-shell singlet state (for M = M′: D_{4h} symmetry, $^1A_{1g}$ state; for M ≠ M′: C_{4v} symmetry, $^1A_1$ state). All DFT results were obtained using the def2-TZVPP basis set. For the CASPT2 calculations, the large ANO-RCC basis was employed (see Computational methods).

Functional	$[Re_2Cl_8]^{2-}$	$[Tc_2Cl_8]^{2-}$	$[Os_2Cl_8]^0$	$[Ru_2Cl_8]^0$	$[Ir_2Cl_8]^{2+}$	$[Rh_2Cl_8]^{2+}$	$[ReTcCl_8]^{2-}$	$[ReOsCl_8]^{1-}$	$[ReIrCl_8]^0$	$[OsIrCl_8]^{1+}$
SVWN	2.202	2.106	2.156	2.246	2.217	2.360	2.400	2.217	2.273	2.325
BP86	2.226	2.132	2.181	2.270	2.245	2.394	2.464	2.241	2.299	2.351
BLYP	2.244	2.152	2.200	2.294	2.271	2.422	2.508	2.263	2.325	2.381
HCTH	2.208	2.108	2.161	2.256	2.227	2.378	2.393	2.226	2.286	2.333
OLYP	2.213	2.116	2.167	2.258	2.227	2.379	2.391	2.230	2.287	2.332
OPBE	2.195	2.096	2.147	2.232	2.198	2.350	2.353	2.209	2.260	2.301
PBE	2.224	2.131	2.179	2.267	2.242	2.391	2.462	2.239	2.296	2.347
B3LYP	2.201	2.096	2.151	2.240	2.201	2.413	2.472	2.218	2.279	2.330
BH&HLYP	2.153	2.034	2.115	2.180	2.117	2.415	2.439	2.192	2.232	2.287
O3LYP	2.194	2.090	2.145	2.233	2.194	2.380	2.452	2.209	2.266	2.309
X3LYP	2.198	2.092	2.147	2.236	2.196	2.413	2.468	2.215	2.274	2.327
TPSS	2.222	2.128	2.177	2.263	2.237	2.391	2.457	2.236	2.292	2.344
VSXC	2.200	2.110	2.157	2.260	2.229	2.401	2.487	2.225	2.289	2.344
TPPSh	2.203	2.103	2.155	2.241	2.207	2.388	2.443	2.217	2.273	2.324
CASPT2(12,12)	2.252									

co-workers,[43] as implemented in the program package MOLCAS, were used in the following contractions: (17s12p5d4f2g) → [5s4p3d1f] for Cl, (24s21p15d11f4g2h) → [8s7p5d3f1g] for Re, Os, Ir, and (21s18p13d6f4g2h) → [7s6p4d2f1g] for Tc, Ru, Rh. These calculations were performed with the program MOLCAS6.[43] The CASPT2 calculations were performed on BP86/TZ2P geometries except for the data presented in Table 1, which are results of geometry optimizations at the CASPT2 level.

In the CASSCF calculations of the $[MM'Cl_8]^x$ systems, we chose active spaces consisting of either eight electrons in eight orbitals, CAS(8,8), or 12 electrons in 12 orbitals, CAS(12,12). The smaller active space formally comprises the *n*dσ, two *n*dπ, and one ndδ metal–metal bonding and antibonding orbitals, whereas the larger active space also includes a metal–ligand σ bonding and antibonding orbital pair. These active spaces can cover static electron correlation effects connected to the metal–metal bond.

To give a balanced description of correlation effects in the calculation of the dissociation of $[MM'Cl_8]^x$ into the D_{4h} symmetric MCl_4^y fragments, the MCl_4^y systems in their $^5A_{1g}$ state were calculated using (4/4) and (6/6) active spaces in the CASSCF. It is, however, important to notice that for systems in which the metal and ligand orbitals interact strongly, e.g., in the case of the cationic system $[Ir_2Cl_8]^{2+}$, the active space has to be considerably larger than (12/12) if one is to calculate dissociation energies, since it is necessary to include the chlorine lone pair orbitals in the active space. As will be discussed later, some of the calculated dissociation energies must therefore be considered with care.

The electronic structure of the $[MM'Cl_8]^x$ molecules was analyzed with various methods. For the charge analysis, we used the natural bond orbital method (NBO) of Weinhold and co-workers[44] as implemented in the Gaussian program.[22] The energy decomposition analysis (EDA)[45–49] calculations have been performed at the BP86 level using uncontracted Slater-type orbitals (STOs), which have TZ2P quality, on geometries optimized at the BP86/TZ2P level.[50] Scalar relativistic effects have been considered using the zero-order regular approximation (ZORA).[51–55] The latter calculations were carried out with the program package ADF.[56,57]

The focus of the EDA[47] is the instantaneous interaction energy, ΔE_{int}, which is the energy difference between the molecule and the fragments with the frozen geometry of the complex. The interaction energy is divided into three main components:

$$\Delta E_{int} = \Delta E_{elstat} + \Delta E_{Pauli} + \Delta E_{orb}$$

The term ΔE_{elstat} gives the electrostatic interaction energy between the fragments, which are calculated with a frozen density distribution in the geometry of the complex. The Pauli repulsion (ΔE_{Pauli}) arises as the energy change associated with the transformation from the superposition of the unperturbed electron densities of fragments $\rho_A + \rho_B$ to the wave function $\Psi^0 = N\hat{A}\{\Psi_A \times \Psi_B\}$, which properly obeys the Pauli principle through explicit antisymmetrization ($\hat{A}$) and renormalization (N) of the product wave function. It comprises the destabilizing interactions between electrons on either fragment with the same spin. The stabilizing orbital interaction term, ΔE_{orb}, is calculated in the final step of

the analysis when the orbitals relax to their final form. The latter can be decomposed into contributions from each irreducible representation of the point group of the interacting system. This is very helpful because it directly gives the stabilization, which comes from orbitals having different symmetry. To obtain the bond dissociation energy, D_e, one has to consider the preparation energy, ΔE_{prep}, which is the energy difference of the fragments between their equilibrium geometry and the geometry that they have in the molecule:

$$\Delta E\,(=-D_e) = \Delta E_{int} + \Delta E_{prep}$$

Performance of DFT functionals

To estimate the performance of the DFT functionals in the description of M–M′ formal quadruple bonds, the species $[Cl_4MM'Cl_4]^x$ (M, M′ = Tc, Re, Ru, Os, Rh, Ir; x = –2, 0, +2) were completely optimized under D_{4h} (C_{4v} in the case of M ≠ M′) symmetry constraint in the $^1A_{1g}$ ($^1A_1$) state at the DFT level using the def2-TZVPP basis set. The optimized metal–metal bond lengths are listed in Table 1.

For the parent compound, $[Re_2Cl_8]^{2-}$, the optimized Re–Re bond length varies considerably between 2.153 Å (BH&HLYP) and 2.244 Å (BLYP), with the experimental value being 2.237(2) Å[3], which is in good agreement with the CASPT2(12,12) result of 2.252 Å and comparable to recently reported DFT values[58] of 2.29, 2.27, and 2.24 Å at the BLYP, PBE, and OPBE level of theory, respectively. In comparison to experiment, the BLYP functional performs best (2.244 Å), followed by BP86 (2.226 Å), PBE (2.224 Å), and TPSS (2.222 Å). This observation also holds for $[Tc_2Cl_8]^{2-}$, where the BLYP value of 2.152 Å is in excellent agreement with the experimental values of 2.147(4)Å[59] and 2.17(1)Å.[60] The BP86 (2.132 Å), PBE (2.131 Å), and TPSS (2.128 Å) results are again very close.

For the other test systems, the M–M′ bond length variation lies between 0.071 and 0.155 Å. BH&HLYP always results in the shortest M–M contacts except for $[Rh_2Cl_8]^{2+}$ and $[ReTcCl_8]^{2-}$, whereas BLYP in all cases gives the longest bonds.

Among the five different types of functionals (LDA, GGA, hybrid-GGA, meta-GGA, hybrid-meta-GGA) there is no clear trend of the accuracy of the calculated bond length. LDA delivers, in all cases, shorter bonds than all GGA functionals, except for OPBE. The GGA functionals are best grouped into two classes: the first one giving longer bonds with the trend PBE < BP86 < BLYP and the second one resulting in shorter bonds with the trend OPBE < HTCH ≈ OLYP. The latter class gives only slightly longer bonds than the hybrid-GGA functionals with a mixing of exact exchange (B3LYP, X3LYP, O3LYP). The general observation that higher amounts of exact exchange lead to shorter bonds also holds in the case of metal–metal bonds as exemplified in the series BLYP > B3LYP > BH&HLYP. The two meta-GGA functionals, TPSS and VSXC, lead to longer bonds than hybrid-GGA functionals, with TPSS being close to the GGA functionals of the first class. Mixing of exact exchange admixture to TPSS, which gives the hybrid-meta-GGA TPSSh, leads to a shortening of the M–M bonds, with the consequence that the performance of TPSSh is comparable to SVWN.

Overall, we conclude that the GGA functionals, BLYP, BP86, PBE, and the meta-GGA functional TPSS deliver acceptable metal–metal bond lengths for the systems under study, irrespective of the metal–metal bond being polar or unpolar, or whether 4d or 5d transition metal atoms are involved. This observation adds to the increasing evidence that GGA functionals perform especially well in the study of transition metal species, as, for example, is summarized in the recent review by Cramer and Truhlar.[61] Also, Cavigliasso and Kaltsoyannis[58] observed that GGAs perform well in the description of structural features of $[M_2Cl_8]^{2-}$ systems. In general, hybrid functionals with more than 5%–15% Hartree–Fock exchange are not capable to describe systems with significant multireference character, as, e.g., is shown by Zhao et al.,[62] and are therefore not suited in the study of systems like the $[MM'Cl_8]^x$ species we are dealing with in this study.

Our main concern, however, is not so much the bond length but the bond dissociation energy (BDE) of the metal–metal formal quadruple bonds. We therefore compared the dissociation energies of the $[MM'Cl_8]^x$ species (M, M′ = Tc, Re, Ru, Os, Rh, Ir; x = –2, 0, +2) for the dissociation in two square planar D_{4h} symmetric $MCl_4^{x/2}$ species in the ($^5A_{1g}$) quintet state. To reduce the influence of structural effects, we based all calculations for a given species on the same geometries, which were optimized at the BP86/TZ2P level. Table 2 gives the results and the following discussion will be based on this. For completeness, Table S1 in the Supplementary data gives the dissociation energies for completely optimized structures at the respective level whose inspection reveals that the geometrical relaxation has no impact on the conclusion presented in the following.

For the parent compound, $[Re_2Cl_8]^{2-}$, we calculate a dissociation energy of D_e = 15.6 kcal/mol at the CASPT2(12,12) level of theory. The comparison with the CASPT2(8,8) result of 17.2 kcal/mol demonstrates that the result can be considered stable with respect to the active space and should thus be a reliable ab initio estimate of the dissociation energy. To the best of our knowledge, there are no reliable experimental values to compare with. The experimental estimate of 152.7 ± 19 kcal/mol is considered "very unreliable".[63] The ab initio, single reference CCSD(T) method underestimates the stability of the Re–Re bond, giving a value of 5.5 kcal/mol. The calculated value at CCSD is D_e = –36.4 kcal/mol (Table 2). The very large contribution from the quasi-perturbative treatment of the connected triple excitations when going from CCSD to CCSD(T) shows that a single configuration wave function method is not appropriate for calculating the bond energy of $[Re_2Cl_8]^{2-}$. Single configuration DFT methods could perform better because of fortuitous error cancellation. However, the DFT results clearly show that the functionals assign stabilities in the wide range from 17.6 kcal/mol (VSXC) to –77.4 kcal/mol (BH&HLYP). There are eight functionals that give negative values for the BDE of $[Re_2Cl_8]^{2-}$. Thus, a careful choice of functional is important for even a qualitatively correct description. Concerning the different types of functionals (LDA, GGA, meta-GGA, meta-hybrid-GGA), one can observe clear trends. The LDA functional SVWN overestimates the stability of the Re–Re

Table 2. Dissociation energy, D_e, in kcal/mol for the dissociation of $[MM'Cl_8]^x$ in the lowest totally symmetric closed-shell singlet state (for M = M′: D_{4h} symmetry, $^1A_{1g}$ state; for M ≠ M′: C_{4v} symmetry, $^1A_1$ state) in two square planar quintet states of D_{4h} symmetry ($^5A_{1g}$). All DFT and coupled cluster results were obtained using the def2-TZVPP basis set. For the CASPT2 calculations, a large ANO-RCC basis was employed (see Computational methods). All geometries were optimized at the BP86/TZ2P level.

Functional	$[Re_2Cl_8]^{2-}$	$[Tc_2Cl_8]^{2-}$	$[Os_2Cl_8]^0$	$[Ru_2Cl_8]^0$	$[Ir_2Cl_8]^{2+}$	$[Rh_2Cl_8]^{2+}$	$[ReTcCl_8]^{2-}$	$[ReOsCl_8]^{1-}$	$[ReIrCl_8]^0$	$[OsIrCl_8]^{1+}$	ΔE^a
SVWN	63.6	38.1	116.2	89.1	3.4	23.5	51.2	147.9	272.7	130.0	45.8
BP86	10.2	–14.3	64.9	39.2	–46.1	–25.7	–1.9	94.7	218.6	78.4	8.4
BLYP	8.9	–17.4	55.7	29.9	–54.7	–38.6	–4.2	90.0	211.3	69.5	12.4
HCTH	–14.0	–38.1	43.9	13.9	–71.0	–60.0	–25.9	72.7	196.9	56.2	29.6
OLYP	–6.7	–34.0	46.1	14.9	–71.0	–60.3	–20.3	77.3	200.1	57.2	26.0
OPBE	–7.4	–34.6	50.3	20.3	–66.9	–55.1	–20.3	79.7	204.8	62.5	23.4
PBE	15.7	–9.2	69.6	43.3	–42.7	–21.9	3.5	99.1	223.9	82.9	6.1
B3LYP	–20.4	–56.9	25.7	–11.1	–69.4	–69.1	–38.3	61.4	190.7	39.7	44.0
BH&HLYP	–77.4	–132.4	–38.4	–92.2	–102.9	–132.6	–105.1	13.7	150.8	–12.6	104.5
O3LYP	–21.4	–54.0	29.2	–5.3	–76.6	–68.2	–37.5	62.7	189.8	41.8	42.2
X3LYP	–21.9	–59.4	23.9	–13.9	–69.3	–69.7	–40.3	60.6	190.3	38.4	45.6
TPSS	6.7	–20.1	59.9	32.4	–49.9	–30.5	–6.4	91.1	215.3	73.4	12.3
VSXC	17.6	–6.7	66.4	41.7	–43.9	–23.3	5.9	95.7	224.5	79.6	8.5
TPPSh	–9.5	–41.6	42.3	10.1	–59.3	–48.3	–25.2	75.8	203.5	56.6	28.8
CCSD	–36.4	–218.6	0.7	–87.9	–74.1	–84.4	–97.7	—[b]	—[b]	—[b]	117.6
CCSD(T)	5.5	–165.3	56.0	—[b]	–3.6	–7.0	–69.3	—[b]	—[b]	—[b]	64.0
CASPT2(8,8)	17.2	–10.0	83.7	75.7	—[c]	—[c]	4.1	102.7	220.1	96.0	5.9
CASPT2(12,12)	15.6	–13.7	77.9	65.4	—[c]	—[c]	3.0	99.6	211.4	83.5	

[a]Average deviation with respect to the CASPT2(12,12) value.

[b]No convergence.

[c]Active space not large enough for the calculation of dissociation energies.

Table 3. Energy lowering of the closed-shell singlet $^1A_{1g}$ ($^1A_1$ for M ≠ M′) state in D_{4h} (C_{4v} for M ≠ M′) symmetry of $[MM'Cl_8]^x$ due to the symmetry breaking unpairing of two electrons leading to open-shell $^1A_1$ biradicals in C_{4v} symmetry. All energies are in kcal/mol and geometries are optimized at BP86/TZ2P.

Functional	$[Re_2Cl_8]^{2-}$	$[Tc_2Cl_8]^{2-}$	$[Os_2Cl_8]^0$	$[Ru_2Cl_8]^0$	$[Rh_2Cl_8]^{2+}$	$[ReTcCl_8]^{2-}$
SVWN	+2.0	+2.3	+2.1	0.0	+2.4	0.0
BP86	–1.4	–2.4	–2.0	–3.3	–0.9	–2.4
BLYP	–1.9	–2.6	–4.2	–4.0	–3.2	–1.7
HCTH	–1.7	–2.3	–2.3	–5.5	–9.1	–3.0
OLYP	–1.1	–2.0	–1.8	–3.9	–8.4	–2.4
OPBE	–1.3	–2.6	–1.2	–1.4	–8.9	–2.7
PBE	–1.1	–2.1	–1.7	–3.1	–0.7	–1.9
B3LYP	–10.5	–13.4	–11.2	–14.5	–10.7	–12.2
BH&HLYP	–29.6	–35.5	–38.7	–39.4	–35.3	–24.6
O3LYP	–6.4	–8.3	–6.7	–9.6	–6.1	–8.3
X3LYP	–11.4	–14.6	–12.6	–17.2	–11.8	–13.4
TPSS	–3.3	–4.7	–3.2	–5.2	–1.9	–4.2
VSXC	–6.9	–7.7	–5.8	–7.4	–3.7	–7.1
TPPSh	–7.7	–10.3	–7.6	–10.9	–6.6	–9.5

bond considerably (D_e = 63.6 kcal/mol), whereas GGA functionals of the first class (PBE, BP86, BLYP) assign values of 15.7, 10.2, and 8.9 kcal/mol, respectively, which are close to the CASPT2(12,12) value. The second class of GGA functionals (HCTH, OLYP, OPBE) underestimates the Re–Re bond stability and leads to even qualitative incorrect D_e values of –14.0, –7.4, and –6.7 kcal/mol, respectively. All hybrid-GGA functionals underestimate the stability considerably with D_e values of –20.4, –21.4, –21.9, and –77.4 kcal/mol for B3LYP, O3LYP, X3LYP, and BH&HLYP, respectively. The meta-GGA functionals, TPPS and VSXC, are comparable to the first class of GGA functionals in their description of the stability of the Re–Re bond, leading to D_e values of 6.7 and 17.6 kcal/mol, respectively. The admixture of exact exchange leads to a decreasing bond stability as exemplified in the series BLYP > B3LYP > BH&HLYP. The same holds for the comparison of the meta-GGA functional TPSS (D_e = 6.7 kcal/mol) with its hybrid congener TPPSh (D_e = –9.5 kcal/mol).

The resulting overall picture for the Re–Re BDE of $[Re_2Cl_8]^{2-}$ is that the first class of GGA functionals (PBE, BP86, BLYP) and the meta-GGA functionals (TPSS and VSXC) give values that are in a reasonably good agreement with the CASPT2(12,12) value, while the other functionals give very poor results.

This conclusion also holds when the remaining $[MM'Cl_8]^x$ systems in our study are considered. For $[Tc_2Cl_8]^{2-}$, e.g., the CASPT2(12,12) D_e value of –13.7 kcal/mol is matched by the GGA functionals BP86 (–14.3 kcal/mol), BLYP (–17.4 kcal/mol), and PBE (–9.2 kcal/mol). The meta-GGA functionals, VSCX and TPSS, are still in reasonable agreement with –6.7 and –20.1 kcal/mol, respectively, whereas all hybrid-GGA functionals, the hybrid-meta-GGA functional, and the second class of GGA functionals underestimate and the LDA overestimates the metal–metal BDE considerably. The CCSD and CCSD(T) values for the BDE of $[Tc_2Cl_8]^{2-}$ are dramatically wrong.

In $[Os_2Cl_8]^0$, we notice a larger difference between the CASPT2(8,8) and the CASPT2(12,12) results, underlining that the metal centered orbitals interact more heavily with the chlorine lone pair orbitals, as discussed above, which leads to a slight imbalance in the correlation energy, which is covered by the active spaces in $[M_2Cl_8]^x$ and the $MCl_4^{x/2}$ fragments. The same holds for $[Ru_2Cl_8]^0$, $[ReIrCl_8]^0$, and $[OsIrCl_8]^{1+}$. We therefore have to assign a larger error bar to the CASPT2(12,12) values of these compounds. For $[Ir_2Cl_8]^{2+}$ and $[Rh_2Cl_8]^{2+}$, it was not possible to design an active space large enough to include all the orbital pairs describing the metal–metal and metal–ligand interactions, so as to obtain a reliable and balanced dissociation energy. This is due to the fact that in these positively charged systems, the metal orbitals contract and lie much deeper than the chlorine lone pair orbitals.

The conclusion is that GGA functionals are able to describe the BDE of metal–metal quadruple bonds with an estimated uncertainty of ±5 kcal/mol, whereas hybrid functionals are not even reliable for qualitative discussions. This observation is in line with the conclusions of numerous DFT validation studies on transition metal compounds as summarized recently by Cramer and Truhlar.[61] The performance of DFT functionals in the studies of M–M bond dissociation energies is normally tested on transition metal dimers, as for these systems experimental data are available. It is therefore interesting to see that the conclusion put forward for such systems, e.g., in refs. 64 and 65, can be carried over to larger systems in which direct, unbridged metal–metal multiple bonds are present. Ab initio calculations must be carried out using multideterminantal methods, as single reference methods, even at CCSD(T), give large errors for D_e.

The natural orbital occupation numbers of the CASSCF wave function for the δ/δ* orbital pair are a measure for the biradical character of the metal–metal bond. The occupation numbers are 1.56/0.44, 1.48/0.52, 1.47/0.53, 1.30/0.70, 1.51/0.49, 1.61/0.39, 1.97/0.03, and 1.95/0.05 in $[Re_2Cl_8]^{2-}$, $[Tc_2Cl_8]^{2-}$, $[Os_2Cl_8]^0$, $[Ru_2Cl_8]^0$, $[ReTcCl_8]^{2-}$, $[ReOsCl_8]^{1-}$, $[ReIrCl_8]^0$, and $[OsIrCl_8]^{1-}$, respectively. This indicates that, except for $[Ru_2Cl_8]^0$, the biradical character of the metal–metal bond is moderate and, thus, closed-shell DFT calculations of singlet species should allow for a qualitative correct

Table 4. Singlet–triplet gap ($^3A_{2u} \leftarrow {}^1A_{1g}$ for M = M′ and $^3A_1 \leftarrow {}^1A_1$ for M ≠ M′) in kcal/mol for $[MM'Cl_8]^x$ in the D_{4h} (C_{4v} for M ≠ M′) symmetric geometry. All DFT results were obtained using the def2-TZVPP basis set. For the CASPT2 calculations, a large ANO-RCC basis was employed (see Computational methods). All geometries were optimized at BP86/TZ2P.

Functional	$[Re_2Cl_8]^{2-}$	$[Tc_2Cl_8]^{2-}$	$[Os_2Cl_8]^{0}$	$[Ru_2Cl_8]^{0}$	$[Ir_2Cl_8]^{2+}$	$[Rh_2Cl_8]^{2+}$	$[ReTcCl_8]^{2-}$	$[ReOsCl_8]^{1-}$	$[ReIrCl_8]^{0}$	$[OsIrCl_8]^{1-}$	ΔE^a
SVWN	8.8	7.8	5.2	3.5	–11.0	6.3	8.4	9.9	16.2	7.6	2.1
BP86	2.8	1.9	0.8	–1.1	–18.8	1.7	2.4	4.6	10.7	2.8	5.9
BLYP	2.9	1.7	0.5	–1.5	–20.5	0.8	2.3	4.4	9.9	2.2	6.0
HCTH	2.9	2.8	1.0	–0.7	–24.1	5.7	2.8	4.8	10.1	2.4	5.6
OLYP	3.5	2.5	1.2	–0.9	–21.7	8.0	3.0	5.2	10.5	2.5	5.6
OPBE	3.8	3.1	1.7	–0.4	–18.1	13.8	3.5	5.7	11.4	3.3	5.2
PBE	3.2	2.3	1.1	–0.8	–18.7	1.9	2.8	5.0	11.0	3.1	5.7
B3LYP	–6.6	–9.0	–8.6	–12.2	–6.9	–9.6	–7.7	–3.6	4.7	–5.2	14.8
BH&HLYP	–23.3	–28.1	–25.3	–32.1	15.1	–39.0	–24.8	–13.8	–3.6	–12.1	29.2
O3LYP	–1.9	–3.5	–3.9	–6.9	–13.1	–4.2	–2.7	0.5	7.3	–1.8	10.4
X3LYP	–7.5	–10.0	–9.5	–13.3	–5.5	–10.7	–8.7	–4.1	4.3	–5.8	15.6
TPSS	1.1	–0.5	–0.8	–3.1	–17.6	0.1	0.3	3.1	9.8	1.6	7.4
VSXC	–2.1	–1.7	–2.7	–3.9	–23.0	–0.9	–1.9	0.7	8.2	0.2	9.2
TPPSh	–3.6	–5.8	–5.4	–8.5	–11.4	–5.1	–4.7	–1.0	7.0	–2.4	11.8
CASPT2(8,8)	9.5	9.1	6.6	6.4	—[b]	—[b]	9.3	9.0	9.5	9.1	0.2
CASPT2(12,12)	9.6	9.1	6.8	6.7	—[b]	—[b]	9.9	9.3	9.6	9.1	

[a]Average deviation with respect to the CASPT2(12,12) value.

[b]Active space is not large enough for the correct description of M–M orbital manifold.

Table 5. Excitation energy from the square planar D_{4h} quintet ($^5A_{1g}$) to the tetrahedral T_d singlet ($^1A_1$) for $[MCl_4]^x$ in kcal/mol. All results were obtained using the def2-TZVPP basis set. All DFT geometries were optimized at the respective level; for the coupled cluster calculations, BP86/TZ2P geometries were used.

Functional	$[ReCl_4]^-$	$[TcCl_4]^-$	$[OsCl_4]^0$	$[RuCl_4]^0$	$[IrCl_4]^+$	$[RhCl_4]^+$	ΔE^a
SVWN	15.9	9.9	–13.9	–19.8	–37.8	–40.9	7.9
BP86	25.3	18.3	–6.0	–12.5	–29.9	–32.9	5.3
BLYP	19.2	13.1	–9.2	–14.7	–30.8	–32.6	7.3
HCTH	29.7	22.9	–4.2	–10.2	–29.1	–30.8	4.8
OLYP	22.8	16.5	–8.0	–13.5	–30.8	–32.4	6.1
OPBE	27.4	20.4	–5.8	–12.2	–30.3	–32.9	4.5
PBE	24.3	17.5	–6.7	–12.9	–30.4	–33.1	5.5
B3LYP	23.7	18.2	–6.6	–12.5	–30.7	–33.1	5.5
BH&HLYP	31.2	27.2	–0.4	–6.4	–29.0	–31.4	5.8
O3LYP	25.2	19.3	–6.6	–12.4	–30.7	–32.8	5.1
X3LYP	23.9	18.9	–6.1	–12.0	–30.4	–32.9	5.4
TPSS	24.7	17.3	–5.2	–12.0	–28.3	–31.3	6.1
VSXC	36.4	30.4	5.2	–1.0	–20.3	–23.0	11.9
TPPSh	27.2	20.2	–3.6	–10.5	–27.8	–31.0	5.9
CCSD	34.0	29.4	–2.2	–10.8	–38.7	–45.6	3.2
CCSD(T)	30.5	25.5	–5.5	–14.4	–36.7	–42.9	

[a]Average deviation with respect to the CCSD(T)/def2-TZVPP value.

description. However, as near degeneracy problems may be better modeled by broken-symmetry DFT approaches, we tested the stability of the closed-shell singlet states towards unpairing of the electron pair in the M–M δ-bonding orbital leading to singlet biradicals with localized, singly occupied d_{xy} metal orbitals. We observed broken-symmetry states for $[Re_2Cl_8]^{2-}$, $[Tc_2Cl_8]^{2-}$, $[Os_2Cl_8]^0$, $[Ru_2Cl_8]^0$, $[Rh_2Cl_8]^{2+}$, and $[ReTcCl_8]^{2-}$, whereas the other systems collapsed to the closed-shell singlet solution. The energy lowering due to the symmetry breaking is given in Table 3. It becomes obvious that, except for SVWN, all functionals predict the biradical state to be energetically favorable. GGA functionals point to a modest stabilization of the biradical state, whereas hybrid functionals give a clear preference for the open-shell singlet states reflecting the general trend that hybrid functionals tend to be favored toward open-shell states. Meta-GGA functionals are between GGA and hybrid functionals.

Related to the stability of the closed singlet state towards the broken-symmetry singlet solution is the question of whether the triplet state, with both the metal–metal δ bonding and antibonding orbitals being singly occupied ($^3A_{2u}$ state in D_{4h} symmetry and $^3A_1$ state in C_{4v} symmetry), is energetically favored over the closed-shell singlet state. In Table 4, we give the $^3A_{2u} \leftarrow {}^1A_{1g}$ adiabatic excitation energy ($^3A_1 \leftarrow {}^1A_1$ in C_{4v} symmetry) for the selected DFT functionals and the CASPT2 model chemistry. The reported splitting for $[Re_2Cl_8]^{2-}$ of 9.6 kcal/mol at the CASPT2 level is in good agreement with former ab initio results, e.g., at the CASPT2 level (9.9 kcal/mol)[66] and at the MRMP2 level (12.0 kcal/mol).[67] For all systems, the singlet–triplet gap is underestimated compared to CASPT2(12,12) by all DFT functionals but SVWN. An exception is $[ReIrCl_8]^0$, where the GGA functionals are in good agreement with the correlated ab initio results. In general, only GGA and LDA functionals give a qualitative correct ordering of states, the singlet state being the ground state. $[ReIrCl_8]^0$ is again an exception. For a quantitative assessment of the electronic states in question, it is clear that no DFT functional provides sufficient reliability.

The above results suggest that (*i*) the conclusion about the performance of the DFT functionals to describe the BDE of metal–metal formal quadruple bonds remains essentially unchanged when considering broken-symmetry states, (*ii*) the natural orbital occupation numbers in the CASSCF point towards small biradical character, and (*iii*) the singlet state is qualitatively correctly assigned to be lower than the triplet state for a chosen subset of functionals. Therefore, it is justified to discuss the bonding situation in the later section on closed-shell singlet calculations with GGA functionals. Furthermore, as both geometries and stabilities of the $[M_2Cl_8]^x$ model systems are reasonably well-described by the GGA functionals, BLYP, PBE, and BP86, these functionals are appropriate for an analysis of the bonding situation.

Comments on the ground state of the MCl_4 fragments

For the d^4-MCl_4^x fragments (M = Tc, Re, Ru, Os, Rh, Ir; $x = -1, 0, +1$), two states must be considered in the quest for the ground state: the square planar quintet state ($^5A_{1g}$ in D_{4h} symmetry) and the tetrahedral singlet state ($^1A_1$ in T_d symmetry). In Table 5, we give the excitation energy $^1A_1 \leftarrow {}^5A_{1g}$ at DFT for a number of functionals and at the CCSD(T) level of theory. The latter is an adequate ab initio method, since the MCl_4^x systems do not exhibit multideterminental character. Qualitatively, all functionals give the correct ground state compared to CCSD(T) except for VSXC, which wrongly predicts that the quintet state is the ground state for $[OsCl_4]^0$. In general, VSXC gives too positive excitation energies, which is probably the consequence of a destabilization of the singlet state. On the other hand, SVWN always gives too negative values, which can be traced back to SVWN underestimating the stability of the quintet state. BH&HLYP, as a third extreme, overestimates the singlet–

triplet gap, probably due to an overstabilization of the quintet state.

Conceptually, two $[MCl_4]^x$ fragments have to be in a quintet state to form a metal–metal quadruple bond. It thus comes as no surprise that the $[ReCl_4]^-$ fragment building the prominent metal–metal quadruple bound $[Re_2Cl_8]^{2-}$ has the largest quintet → singlet gap (30.5 kcal/mol) and is thus ideally suited for the quadruple metal–metal bond. Except for the Re and Tc species, all MCl_4^x fragments have singlet ground states and rather large singlet → quintet gaps. Only if the metal–metal bond strength overcomes this excitation energy, stable compounds with metal–metal quadruple bonds may be expected.

Analysis of the metal–metal bonding situation

To obtain a thorough understanding of the metal–metal quadruple bond in the $(d–d)^8$ systems $[MM'Cl_8]^x$, we start with a qualitative discussion of the orbitals involved in this bonding. Figure 1 serves as an illustration for this purpose.

For each M–M′ bond in question one must, in principle, consider four orbitals of different character. Depending on whether it is metal–metal bonding or antibonding and whether it is metal–ligand bonding or antibonding, one obtains (a) one metal–ligand bonding/metal–metal bonding orbital, (b) one metal–ligand bonding/metal–metal antibonding orbital, (c) one metal–ligand antibonding/metal–metal bonding orbital, and (d) one metal–ligand antibonding/metal–metal antibonding orbital.

In the case of the metal–metal δ bond in $[MM'Cl_8]^x$, these four orbitals are (Fig. 1) the $1b_{2g}$ orbital as component (a), the $1b_{1u}$ orbital as component (b), the $2b_{2g}$ orbital as component (c), and the $2b_{1u}$ orbital as component (d).

The discussion of the metal–metal bond usually considers only the pair of the metal–ligand antibonding orbitals (c) and (d). This is reasonable in cases where the metal orbitals lie considerably higher in energy than the ligand orbitals or where the metal–ligand overlap is poor. For the metal–metal δ bond in the $[Re_2Cl_8]^{2-}$ system, the orbitals of type (c) and (d) are basically metal orbitals (65% metal character)[68] with small contributions from the chlorine atoms, whereas the fully occupied and energetically much lower lying orbitals of type (a) and (b) are mainly ligand orbitals with only 33% and 24% contribution of the Re atomic orbitals, respectively. If, however, the size of the metal atom decreases and the metal orbitals are energetically more stabilized as in $[Os_2Cl_8]^0$ and $[Ir_2Cl_8]^{2+}$, the metal atom contribution of the completely occupied orbitals (a) and (b) increases; for the metal–metal δ bond in $[Os_2Cl_8]^0$ to 50% and 44%, for (a) and (b), respectively, and for $[Ir_2Cl_8]^{2+}$ to 59% and 58% for (a) and (b), respectively. The metal contribution to the occupied metal–metal bonding orbital of type (c) decreases once the metal orbitals contract and become energetically stabilized. Since orbitals (a) and (c) are metal–metal bonding and orbital (b) is metal–metal antibonding, the net metal–metal bond order is thus smaller if the metal orbitals contract and become energetically stabilized, as is the case for $[Os_2Cl_8]^0$ and $[Ir_2Cl_8]^{2+}$. This qualitative insight is corroborated by numerical results. The Wiberg bond order at BP86/def2-TZVPP//BP86/TZ2P for the metal–metal bond decreases in the order of 2.41, 1.55, and 0.77 for $[Re_2Cl_8]^{2-}$, $[Os_2Cl_8]^0$, and $[Ir_2Cl_8]^{2+}$, respectively. Likewise, the occupation of the metal-d_{xy} orbital, as given by the natural population analysis at BP86/def2-TZVPP//BP86/TZ2P, increases in the order of 1.30, 1.51, and 1.65 e for $[Re_2Cl_8]^{2-}$, $[Os_2Cl_8]^0$, and $[Ir_2Cl_8]^{2+}$, respectively, reflecting the higher metal character of the two low lying, occupied metal–metal bonding and antibonding orbitals of type (a) and (b), respectively.

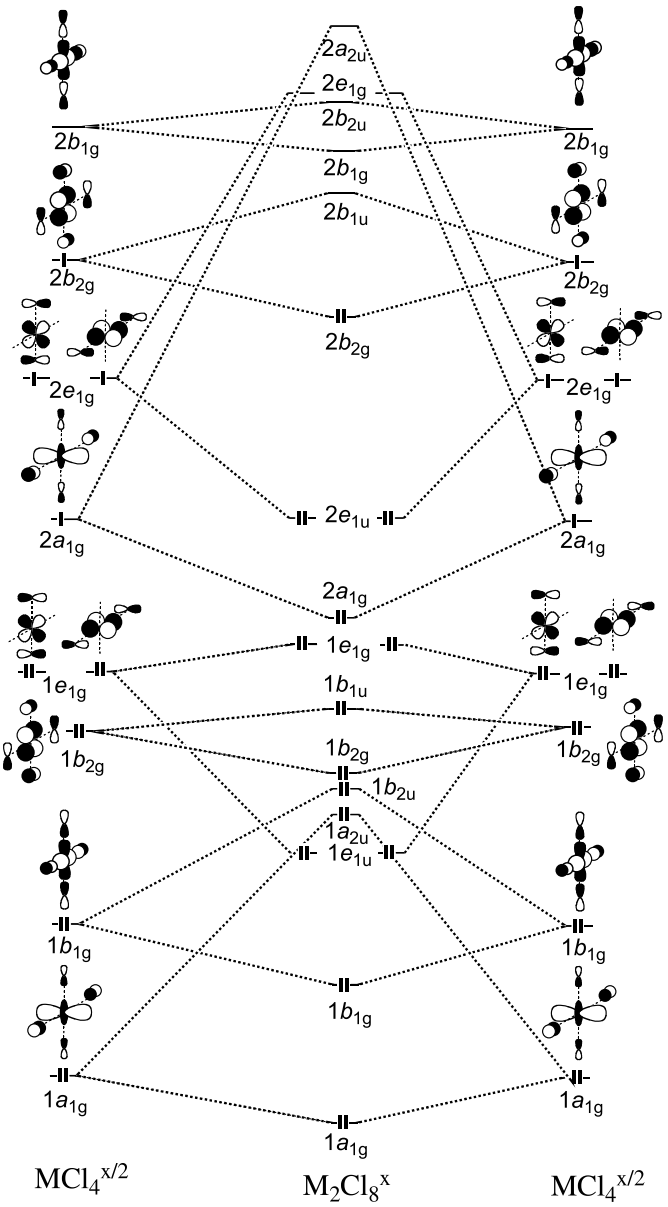

Fig. 1. Schematic molecular orbital interaction diagram for two d^4-$MCl_4^{x/2}$ fragments building a D_{4h} symmetric $[M_2Cl_8]^x$ complex.

Tables 6–9 give the results of the energy decomposition analysis (EDA) and the population analysis data (partial charges, q, orbital occupation numbers, n, and Wiberg bond indices, P) for $[MM'Cl_8]^x$ (M, M′ = Tc, Re, Ru, Os, Rh, Ir; x = –2, –1, 0, +1, +2). For the EDA, we chose C_{4v} symmetric MCl_4^y species in the $^5A_1$ state as interacting fragments, which corresponds to a formal d-electron distribution of $d_{z^2}{}^1$, $d_{xz}{}^1$, $d_{yz}{}^1$, $d_{xy}{}^1$, and $d_{x^2-y^2}{}^0$ at the metal atoms.

Table 6. Energy decomposition analysis for the D_{4h} symmetric $M_2Cl_8^x$ (M = Tc, Re, Ru, Os, Rh, Ir; x = –2, 0, +2) under C_{4v} symmetry at BP86/TZ2P. MCl_4^y (y = –1, 0, +1) in the quintet $^5A_1$ state were used as fragments. Optimized metal–metal distances (R, in Å), NBO partial charge of the metal atom and of the $MCl_4^{x/2}$ fragment (q), occupation of the d_{xy} orbital of the metal atom (n), as well as the Wiberg bond index of the M–M pair (P) are also given. The latter population analysis data are given at BP86/def2-TZVPP//BP86/TZ2P.

	$[Re_2Cl_8]^{2-}$	$[Tc_2Cl_8]^{2-}$	$[Os_2Cl_8]^0$	$[Ru_2Cl_8]^0$	$[Ir_2Cl_8]^{2+}$	$[Rh_2Cl_8]^{2+}$
ΔE_{int}	–54.2	–22.2	–92.8	–56.2	3.5	19.0
ΔE_{Pauli}	404.9	338.3	256.7	187.6	162.4	161.3
ΔE_{elstat}[a]	–244.1 (53.2%)	–162.9 (45.2%)	–151.7 (43.4%)	–88.7 (36.4%)	30.5 (<0.0%)	41.3 (<0.0%)
ΔE_{orb}[a]	–214.9 (46.8%)	–197.6 (54.8%)	–197.8 (56.6%)	–155.1 (63.6%)	–189.5 (100.0%)	–183.6 (100.0%)
Δa_1 (σ,δ)[b]	–84.4 (39.3%)	–78.6 (39.8%)	–97.6 (49.3%)	–81.6 (52.6%)	–102.6 (54.1%)	–88.1 (48.0%)
Δa_2[b]	–0.1 (0.1%)	–0.1 (0.1%)	–0.1 (<0.1%)	–0.1 (0.1%)	–0.6 (0.3%)	–0.8 (0.5%)
Δb_1[b]	–1.4 (0.7%)	–2.1 (1.0%)	–2.9 (1.5%)	–2.8 (1.8%)	–4.1 (2.1%)	–4.1 (2.2%)
Δb_2 (δ)[b]	–0.5 (0.2%)	2.4 (<0.0%)	0.9 (<0.0%)	4.1 (<0.0%)	–0.6 (0.3%)	–1.2 (0.6%)
Δe (π)[b]	–128.5 (59.8%)	–119.2 (60.3%)	–98.2 (49.6%)	–74.6 (48.1%)	–81.7 (43.1%)	–89.4 (48.7%)
ΔE_{prep}[c]	36.7	38.7	33.0	33.1	37.7	40.2
D_e	17.5	–16.5	59.8	23.1	–41.2	–59.2
n(M[d_{xy}])	1.30	1.33	1.51	1.53	1.65	1.66
q(M)	0.55	0.45	0.56	0.39	0.59	0.45
q(MCl_4)	–1.0	–1.0	0.00	0.00	1.00	1.00
P(M–M)	2.41	2.30	1.55	1.30	0.77	0.58
R(M–M)	2.231	2.152	2.273	2.263	2.438	2.464

[a]Values in parentheses give the percentage contribution to the total attractive interactions, $\Delta E_{elstat} + \Delta E_{orb}$.

[b]Values in parentheses give the percentage contribution to the total orbital interactions, ΔE_{orb}.

[c]Fragments relax into a tetrahedrally distorted square planar quintet of D_{2d} symmetry.

Table 6 shows that, in the parent compound $[Re_2Cl_8]^{2-}$, the major stabilizing contribution to the total interaction energy, ΔE_{int} = –54.2 kcal/mol, is due to the classical electrostatic contribution (53.2% of the stabilizing terms), whereas the orbital (covalent) interaction contributes 46.8%.[69] This observation is somewhat surprising, given the fact that two negatively charged moieties, $ReCl_4^-$, interact. One would intuitively assume to observe a net electrostatic repulsion. Such an assumption is not justified because the charge distribution in the atomic basins is highly anisotropic. The rhenium atoms carry a positive charge of +0.55 e but the attraction of the singly occupied metal d_{z^2} orbital of one Re atom by the nucleus of the other Re atom yields a strong electrostatic attraction.[70] Note that even nonpolar bonds are, in most cases, stabilized by classical electrostatic contributions.[71,72] The very large Pauli repulsion between the two fragments of 404.9 kcal/mol compensates to a large extent for the stabilizing electrostatic and orbital contributions. The attractive orbital contributions result mainly from orbitals of e (π) symmetry (59.8% of the total orbital interaction), followed by orbitals of $a_1(\sigma)$ symmetry with 39.3%. Interestingly, the δ bonding orbitals in b_2 symmetry do not seem to be of importance for the covalent stabilization, as they contribute only 0.2% to the total ΔE_{orb}.

Comparing the former results with the 4d transition metal congener $[Tc_2Cl_8]^{2-}$, one notices some similarities but also a significant difference. A steep decrease in the electrostatic attraction is responsible for the overall instability of $[Tc_2Cl_8]^{2-}$. The drop in the ΔE_{elstat} contribution can be explained by two factors. On the one hand, the Tc orbitals are more compact than the Re orbitals, leading to a reduced net attraction of the electrons in this orbital by the opposing metal nucleus. On the other hand, the Tc atom has a lower positive charge (+0.45 e) than the Re atom (+0.55 e), meaning that the positive charge of the nucleus is screened more effectively in the Tc compound. The increased electron density on Tc can be rationalized based on the qualitative bonding picture developed above and noticing that the Tc atomic orbitals are more compact and lie energetically below the Re atomic orbitals (see, e.g., the discussion in ref. 73). The details of the covalent contributions to the bond energy remain unchanged compared to the Re compound, with the e (π) term (60.3%) exceeding the $a_1(\sigma)$ contribution (39.8%). The similarity in the covalent bonding contribution is also reflected in the comparable Wiberg bond indices of 2.41 and 2.30 for the Re and the Tc complexes, respectively. It is interesting to notice that the intrinsic bond strength, as measured by the interaction energy, ΔE_{int}, is still stabilizing (–22.2 kcal/mol). This, however, is not sufficient to overcompensate the preparation energy of ΔE_{prep} = 38.7 kcal/mol, which is needed for the deformation of the $[TcCl_4]^-$ fragments from their relaxed geometry to the structure that they adopt to interact.

The M–M bond in $[Os_2Cl_8]^0$ is considerably stronger than in its group 7 isoelectronic congener, $[Re_2Cl_8]^{2-}$. This is indicated by the interaction energy, which amounts to –92.8 kcal/mol in the former compared to –54.2 kcal/mol in the latter. The absolute values of the individual contributions to ΔE_{int}, however, are smaller. The main reason for the higher stability of $[Os_2Cl_8]^0$ is the steep decrease of the Pauli repulsion, an effect that is clearly related to the reduced net charge of the complex. A similar behavior was observed and discussed in ref. 69 for $[Re_2Cl_8]^{2-}$ and $[Re_2Cl_8]^0$. Interestingly, the absolute values of the electrostatic and the orbital contributions are very similar for the $[Os_2Cl_8]^0$ and the $[Tc_2Cl_8]^{2-}$ complexes, suggesting a very similar bonding picture. This is misleading though, since the π orbital contributions are reduced to 49.6% and the σ orbital contributions are enhanced

Table 7. Energy decomposition analysis for the C_{4v} symmetric $[MM'Cl_8]^x$ (M, M′ = Tc, Re, Ru, Os, Rh, Ir; x = –1, 0, +1) at BP86/TZ2P. MCl_4^y (y = –1, 0, +1) in the quintet $^5A_1$ state were used as fragments. Optimized metal–metal distances (R) in Å, the Wiberg bond index of the M–M′ pair (P), the change in the orbital occupation (Δn), and the change in partial charge (Δq) relative to the homodimetallic systems are also given. The population analysis data are given at BP86/def2-TZVPP//BP86/TZ2P.

	$[ReOsCl_8]^{1-}$		$[ReIrCl_8]^0$		$[OsIrCl_8]^{1+}$		$[TcRuCl_8]^{-1}$		$[TcRhCl_8]^0$		$[RuRhCl_8]^{1+}$	
ΔE_{int}	–132.0		–247.4		–95.3		–95.4		–207.9		–66.8	
ΔE_{Pauli}	335.8		270.8		196.5		261.2		196.3		159.8	
ΔE_{Elstat}[a]	–239.6 (51.2%)		–255.1 (49.2%)		–93.4 (32.0%)		–162.7 (45.6%)		–188.7 (46.7%)		–58.7 (25.9%)	
ΔE_{orb}[a]	–228.2 (48.8%)		–263.1 (50.8%)		–198.4 (67.8%)		–193.9 (54.4%)		–215.5 (53.3%)		–167.9 (74.1%)	
Δa_1 (σ,δ)[b]	–92.4 (40.5%)		–98.6 (37.5%)		–100.4 (50.6%)		–80.7 (41.7%)		–82.0 (38.0%)		–82.3 (49.0%)	
Δa_2[b]	–0.1 (<0.1%)		–0.3 (0.1%)		–0.3 (0.1%)		–0.1 (0.1%)		–0.3 (0.1%)		–0.4 (0.2%)	
Δb_1[b]	–2.5 (1.1%)		–4.1 (1.6%)		–3.7 (1.9%)		–2.9 (1.5%)		–4.1 (1.9%)		–3.4 (2.1%)	
Δb_2 (δ)[b]	–10.4 (4.6%)		–41.1 (15.6%)		–10.1 (5.1%)		–6.8 (3.5%)		–37.5 (17.4%)		–8.1 (4.9%)	
Δe (π)[b]	–122.8 (53.8%)		–119.1 (45.3%)		–83.9 (42.3%)		–103.3 (53.3%)		–91.7 (42.6%)		–73.7 (43.9%)	
ΔE_{prep}[c]	37.3		41.9		33.7		38.7		39.9		33.9	
D_e	94.7		205.5		61.6		56.7		168.0		32.9	
M	Re	Os	Re	Ir	Os	Ir	Tc	Ru	Tc	Rh	Ru	Rh
$\Delta n(d_{xy})$	–0.09	0.08	–0.19	0.20	–0.11	0.11	–0.09	0.10	–0.19	0.20	–0.13	0.11
Δq(M)	0.02	0.01	0.02	0.02	–0.04	0.04	–0.02	0.03	–0.11	0.06	–0.08	0.03
$\Delta q(MCl_4)$	0.61	–0.61	1.30	–1.30	0.64	–0.64	0.65	–0.65	1.25	–1.25	0.61	–0.61
P(M–M′)	1.94		1.36		1.08		1.74		1.11		0.82	
R(M–M′)	2.245		2.300		2.352		2.195		2.299		2.395	

[a]Values in parentheses give the percentage contribution to the total attractive interactions, $\Delta E_{elstat} + \Delta E_{orb}$.
[b]Values in parentheses give the percentage contribution to the total orbital interactions, ΔE_{orb}.
[c]Fragments relax into a tetrahedrally distorted square planar quintet of D_{2d} symmetry.

Table 8. Energy decomposition analysis for the C_{4v} symmetric $[MM'Cl_8]^x$ (M, M′ = Tc, Re, Ru, Os, Rh, Ir; x = –1, 0, +1) at BP86/TZ2P. MCl_4^y (y = –1, 0, +1) in the quintet $^5A_1$ state were used as fragments. Optimized metal–metal distances (R) in Å, the Wiberg bond index of the M–M′ pair (P), the change in the orbital occupation (Δn), and the change in partial charge (Δq) relative to the homodimetallic systems are also given. The population analysis data are given at BP86/def2-TZVPP//BP86/TZ2P.

	$[ReRuCl_8]^{1-}$		$[ReRhCl_8]^0$		$[OsRhCl_8]^{1+}$		$[TcOsCl_8]^{-1}$		$[TcIrCl_8]^0$		$[RuIrCl_8]^{1+}$	
ΔE_{int}	–119.9		–238.0		–84.3		–106.9		–216.2		–75.0	
ΔE_{Pauli}	290.9		221.3		168.0		299.1		236.5		172.7	
ΔE_{elstat}[a]	–194.2 (47.3%)		–213.0 (46.4%)		–69.0 (27.3%)		–199.9 (49.2%)		–221.5 (48.9%)		–70.8 (28.6%)	
ΔE_{orb}[a]	–216.6 (52.7%)		–246.4 (53.6%)		–183.3 (72.7%)		–206.0 (50.8%)		–231.2 (51.1%)		–176.8 (71.4%)	
Δa_1 (σ,δ)[b]	–85.4 (39.4%)		–86.0 (34.9%)		–88.0 (48.0%)		–87.6 (42.5%)		–93.9 (40.6%)		–93.2 (52.7%)	
Δa_2[b]	–0.1 (0.1%)		–0.3 (0.1%)		–0.3 (0.2%)		–0.1 (0.0%)		–0.3 (0.1%)		–0.3 (0.2%)	
Δb_1[b]	–2.6 (1.2%)		–3.9 (1.6%)		–3.4 (1.9%)		–2.8 (1.4%)		–4.3 (1.9%)		–3.6 (2.0%)	
Δb_2 (δ)[b]	–13.2 (6.1%)		–48.6 (19.7%)		–15.6 (8.5%)		–4.6 (2.2%)		–30.2 (13.1%)		–3.5 (2.0%)	
Δe (π)[b]	–115.3 (53.2%)		–107.6 (43.7%)		–75.9 (41.4%)		–111.0 (53.9%)		–102.6 (44.4%)		–76.2 (43.1%)	
ΔE_{prep}[c]	38.8		41.5		33.1		36.9		40.4		33.8	
D_e	81.1		196.5		51.2		70.0		175.8		41.2	
M	Re	Ru	Re	Rh	Os	Rh	Tc	Os	Tc	Ir	Ru	Ir
$\Delta n(d_{xy})$	–0.13	0.13	–0.21	0.22	–0.17	0.15	–0.07	0.07	–0.15	0.17	–0.07	0.06
Δq(M)	0.12	–0.06	0.03	0.02	–0.04	0.01	–0.08	0.06	–0.13	0.08	–0.09	0.06
$\Delta q(MCl_4)$	0.86	–0.86	1.43	–1.43	0.77	–0.77	0.46	–0.46	1.11	–1.11	0.46	–0.46
P(M–M)	1.79		1.18		0.91		1.86		1.29		0.97	
R(M–M)	2.219		2.297		2.275		2.222		2.296		2.371	

[a]Values in parentheses give the percentage contribution to the total attractive interactions, $\Delta E_{elstat} + \Delta E_{orb}$.
[b]Values in parentheses give the percentage contribution to the total orbital interactions, ΔE_{orb}.
[c]Fragments relax into a tetrahedrally distorted square planar quintet of D_{2d} symmetry.

to 49.3% of the total ΔE_{orb} in the Os compound. The reduced π contribution can be explained by the reduced overlap between the fragment π orbitals with overlap integrals of 0.21, 0.18, and 0.14 in the Re, Tc, and Os compounds, respectively. This is a consequence of the decreasing size of the metal orbitals with decreasing negative charge and (or) decreasing row in the periodic system.

The nonclassical interaction between the fragments building the group 8 compound $[Ir_2Cl_8]^{2+}$ is not strong enough to compensate for their electrostatic repulsion of 30.5 kcal/mol

Table 9. Energy decomposition analysis for the C_{4v} symmetric $[MM'Cl_8]^x$ (M, M′ = Tc, Re, Ru, Os, Rh, Ir; x = –2, 0, +2) at BP86/TZ2P. MCl_4^y (y = –1, 0, +1) in the quintet $^5A_1$ state were used as fragments. Optimized metal–metal distances (R) in Å, the Wiberg bond index of the M–M′ pair (P), the change in the orbital occupation (Δn), and the change in partial charge (Δq) relative to the homodimetallic systems are also given. The population analysis data are given at BP86/def2-TZVPP//BP86/TZ2P.

	$[ReTcCl_8]^{2-}$		$[OsRuCl_8]^0$		$[IrRhCl_8]^{2+}$	
ΔE_{int}	–37.9		–73.9		12.0	
ΔE_{Pauli}	367.8		217.3		156.7	
ΔE_{elstat}[a]	–199.3 (49.1%)		–115.2 (39.6%)		40.0 (0.0%)	
ΔE_{orb}[a]	–206.4 (50.9%)		–176.0 (60.4%)		–184.7 (100.0%)	
Δa_1 (σ,δ)[b]	–81.4 (39.5%)		–89.4 (50.1%)		–94.5 (51.2%)	
Δa_2[b]	–0.1 (0.1%)		–0.1 (0.1%)		–0.7 (0.4%)	
Δb_1[b]	–1.7 (0.8%)		–2.9 (1.6%)		–4.0 (2.2%)	
Δb_2 (δ)[b]	0.7 (<0.0%)		2.0 (<0.0%)		–1.5 (0.1%)	
Δe (π)[b]	–123.9 (60.0%)		–85.7 (48.7%)		–84.0 (45.5%)	
ΔE_{prep}[c]	38.7		33.0		39.0	
D_e	0.4		40.9		–51.0	
M	Re	Tc	Os	Ru	Ir	Rh
$\Delta n(d_{xy})$	–0.03	0.03	–0.04	0.03	–0.06	0.05
Δq(M)	0.12	–0.10	0.04	–0.04	0.00	–0.02
$\Delta q(MCl_4)$	0.20	–0.20	0.17	–0.17	0.13	–0.13
P(M–M)	2.35		1.42		0.66	
R(M–M)	2.193		2.265		2.454	

[a]Values in parentheses give the percentage contribution to the total attractive interactions, $\Delta E_{elstat} + \Delta E_{orb}$.

[b]Values in parentheses give the percentage contribution to the total orbital interactions, ΔE_{orb}.

[c]Fragments relax into a tetrahedrally distorted square planar quintet of D_{2d} symmetry.

and the Pauli repulsion of 162.4 kcal/mol. The resulting total interaction energy of 3.5 kcal/mol is destabilizing. The size of the orbital interaction term should be regarded with some care, as the singly occupied fragment orbitals, whose coupling is mainly responsible for this energy lowering, have some ligand character in the case of $[Ir_2Cl_8]^{2+}$, as was discussed in the beginning of the section in connection with Fig. 1. The ΔE_{orb} term should thus not be identified with the pure M–M interaction, but contains a mixture of metal–metal, metal–ligand, and eventually also ligand–ligand interactions. This argument is supported by the considerably smaller Wiberg bond index of 0.77 for $[Ir_2Cl_8]^{2+}$ compared to 1.55 for $[Os_2Cl_8]^0$, whereas the difference between the ΔE_{orb} values of the Os compound (–197.8 kcal/mol) and the Ir species (–189.5 kcal/mol) is relatively low and blurs, to a certain degree, the difference in the bonding pattern.

The difference between $[Os_2Cl_8]^0$ and its lighter analogue $[Ru_2Cl_8]^0$ is comparable to the difference between $[Re_2Cl_8]^{2-}$ and $[Tc_2Cl_8]^{2-}$. The change from a 5d to a 4d metal weakens the metal–metal interaction considerably, due to the reduction in size of the metal orbitals. This reduction leads to a decreased overlap between the metal orbitals, to which the system can answer by a decrease in the central metal–metal bond length, but only to a limited degree, since an increased ligand–ligand repulsion counterbalances this process. The strong decrease in the electrostatic contribution in the 4d systems can also be attributed to the more compact orbitals of the 4d metal atoms.

Comparing the analysis results for $[M_2Cl_8]^{2-}$ with the ones for $[M_2Cl_8]^0$ and for $[M_2Cl_8]^{2+}$ shows that the uncharged species are the most stable, followed by the negatively charged ones, with the positively charged systems being unstable. The lower bond strength of $[M_2Cl_8]^{2-}$ is due to a very high Pauli repulsion, whereas the positively charged species are destabilized by classical electrostatic repulsion. In all cases, the δ bonding orbitals are of no importance for the bond strength, whereas the π orbitals dominate the covalent contribution for the negatively charged species and the σ contribution is more important for the remaining compounds.

The EDA results for some heteronuclear compounds, $[MM'Cl_8]^x$ (M = Tc, Re, Ru, Os, Rh, Ir; x = –2, 0, +2), are given in Table 9. These compounds are species in which two metal atoms of the same group, but of different rows in the periodic table, interact with each other. The comparison with the corresponding homodinuclear systems reveals that all bond energy contributions are halfway between the homonuclear values. The bonding situation does thus not change from the homo- to the hetero-dinuclear systems and thus, the polarity of the metal–metal bond appears to be low. The partial charges support this finding as the charge transfer between the two different MCl_4^x units is small ($|\Delta q(MCl_4^x)|$ between 0.13–0.20 e) with the charge of the metal atoms being essentially unchanged. The picture does change for the heterodimetallic systems with metal atoms of the same row but of different groups in the periodic table (Table 7). In this case, the intrinsic bond strength is considerably enhanced compared to the corresponding nonpolar compounds. For example, $[ReOsCl_8]^{1-}$ has an intrinsic bond strength of –132.0 kcal/mol, while for $[Re_2Cl_8]^{2-}$ ΔE_{int} amounts to –54.2 kcal/mol and for $[Os_2Cl_8]^0$ to –92.8 kcal/mol. The main reason for this observation is that the Pauli repulsion is considerably weaker compared to the dianionic Re system, while the classical electrostatic interaction in the monoanionic system is increased compared to the neutral Os system. The covalent bonding does not dramatically change; the π bonding remains the dominating contribution to ΔE_{orb} (53.8%). There is, however, an increase in the contribution due to the b_2 (δ) orbitals of 4.6%. We attribute a part of this energy gain to a charge transfer from the δ orbitals of $ReCl_4^-$ to the δ orbitals of the $OsCl_4^0$ fragment, since the d_{xy} orbital of Re looses 0.1 e to the Os d_{xy} orbital (Table 7). The overall charge transfer from the $ReCl_4^-$ onto the $OsCl_4^0$ moiety is considerable with 0.61 e, but the partial charge of the metal atoms remains virtually constant. A similar interpretation can be given to the $[ReIrCl_8]^0$ system, where the two oppositely charged fragments, $ReCl_4^-$ and $IrCl_4^+$, interact, which leads to an exceptionally large electrostatic contribution of –255.1 kcal/mol. The charge transfer in this system is large with 1.30 e, while the metal atom partial charge changes very little. As in the former case, charge transfer between the d_{xy} orbitals of the two metal atoms of 0.2 e leads to a large energy contribution in the Δb_2 term. The combination of the group 8 metal Os with the group 9 metal Ir leads to the cationic $[OsIrCl_8]^+$ system, which also has an increased stability compared to both homodimetallic analogues, which is interesting as $[Ir_2Cl_8]^{2+}$ is unstable. The

much more favorable electrostatic interaction between a neutral and a cationic system compared to the one between two cations is the main reason for this observation.

For the combination of two 4d metals of different rows in the periodic table (Table 7), the same bonding picture emerges as for the 5d metals. The polar metal–metal bonds show an increased stability compared to the homodinuclear counterparts, mainly due to a reduced Pauli repulsion, more favorable electrostatic interactions, and charge transfer.

Table 8 shows the analysis results for heterodinuclear compounds with metal atoms of different groups and different rows in the periodic table. Also in this case, the stability of the metal–metal bond increases compared to the unpolar situation, but the bonding situation of the two systems is very similar. However, the charge transfer contribution as measured by $|\Delta q(MCl_4)|$ increases whenever the 5d moiety is more negatively charged than the 4d moiety, compared to the 5d–5d analogues. On the other hand, a 4d MCl_4^x fragment that is more negatively charged than the 5d fragment interacts and loses fewer electrons than it would when combined with a 4d fragment. This is exemplified by the systems $[TcOsCl_8]^{1-}$ with $|\Delta q(MCl_4)| = 0.47$ and $[TcRuCl_8]^{1-}$ with $|\Delta q(MCl_4)| = 0.65$. This means that there is a better "match" if the M–M bond is built between a 4d metal of a lower group number than the 5d metal ("early 4d–late 5d"). We note that the charge transfer trends are reflected in the trends of the Δb_2 (δ) contributions to the orbital interaction energy in the EDA. Furthermore, the size of the bond order as measured by the Wiberg bond index also follows this matching rule.

Summary

The study of the bonding situation in the formally quadruply bonded $(d–d)^8$ $[MM'Cl_8]^x$ compounds and the test of the performance of DFT functionals can be summarized as follows: (*i*) The GGA functionals BLYP, BP86, and PBE, show the best performance when it comes to structure prediction and in the description of the dissociation energies. We estimate these functionals to deliver dissociation energies within ±5 kcal/mol from the CASPT2 results. (*ii*) Hybrid functionals are not to be used for compounds of the type discussed here as they lead to increasingly too short and too weak bonds with the amount of exact exchange included. (*iii*) The ground state of the MCl_4^y fragments can either be a D_{4h} symmetric quintet or a T_d symmetric singlet state. Most of the studied fragments have a singlet ground state with the exception of $ReCl_4^-$ and $TcCl_4^-$. Since the quintet state is the valence state for building a metal–metal quadruple bond, this finding can serve as an explanation for the difficulties to isolate more metal–metal multiply bonded systems. (*iv*) The strength of unpolar metal–metal bonds is reduced in going from group 7 metals to group 8 metals and to group 9 metals. 4d transition metal atoms form weaker metal–metal bonds than 5d species. (*v*) The instrinsic bond strength in the unpolar systems is in approximately equal parts due to orbital interactions and classical electrostatic contributions. The π orbitals dominate the orbital interaction, while δ orbitals are of minor importance. (*vi*) Polar metal–metal bonds show enhanced bond strength compared to unpolar bonds due to a reduced Pauli repulsion, more favorable classical electrostatics interactions, and charge transfer. 5d–5d metal atom pairs form the most stable polar metal–metal bonds. The charge transfer is small in a heterodimetallic system with two metal atoms of the same group and it is large if the two metal atoms have considerably different size as, e.g., in a system in which a more negatively charged 5d metal fragment interacts with a more positively charged 4d metal fragment.

The knowledge on the performance of the DFT functionals will be useful in the study of more complex systems, e.g., the Por–M–M′–Por systems of Collmann, which will be the subject of further studies. The insight into the bonding situation of metal–metal bonded systems should be helpful in the design of new polar metal–metal bonded systems.

Supplementary data

Supplementary data for this article are available on the journal Web site (canjchem.nrc.ca).

Acknowledgment

This work was supported by the Deutsche Forschungsgemeinschaft.

References

(1) (a) Cotton, F. A.; Harris, C. B. *Inorg. Chem.* **1965**, *4* (3), 330. doi:10.1021/ic50025a015.; (b) Cotton, F. A. *Inorg. Chem.* **1965**, *4* (3), 334. doi:10.1021/ic50025a016.

(2) (a) Poineau, F.; Gagliardi, L.; Forster, P. M.; Sattelberger, A. P.; Czerwinski, K. R. *Dalton Trans.* **2009**, 5954. doi:10.1039/b902106j. PMID:19623396.; (b) Wang, X.-B.; Wang, L.-S. *J. Am. Chem. Soc.* **2000**, *122* (9), 2096. doi:10.1021/ja994200q.

(3) Cotton, F. A.; Murillo, C. A.; Walton, R. A. *Multiple Bonds Between Metal Atoms,* 3rd ed.; Springer Science and Business Media, Inc.: New York, 2005.

(4) Nguyen, T.; Sutton, A. D.; Brynda, M.; Fettinger, J. C.; Long, G. J.; Power, P. P. *Science* **2005**, *310* (5749), 844. doi:10.1126/science.1116789. PMID:16179432.

(5) (a) Gagliardi, L.; Roos, B. O. *Nature* **2005**, *433* (7028), 848. doi:10.1038/nature03249. PMID:15729337.; (b) Roos, B. O.; Borin, A. C.; Gagliardi, L. *Angew. Chem. Int. Ed.* **2007**, *46* (9), 1469. doi:10.1002/anie.200603600.; (c) Roos, B. O.; Malmqvist, P.-Å.; Gagliardi, L. *J. Am. Chem. Soc.* **2006**, *128* (51), 17000. doi:10.1021/ja066615z. PMID:17177451.

(6) (a) Kreisel, K. A.; Yap, G. P. A.; Dmitrenko, O.; Landis, C. R.; Theopold, K. H. *J. Am. Chem. Soc.* **2007**, *129* (46), 14162. doi:10.1021/ja076356t. PMID:17967028.; (b) Noor, A.; Wagner, F. R.; Kempe, R. *Angew. Chem. Int. Ed.* **2008**, *47* (38), 7246. doi:10.1002/anie.200801160.; (c) Tsai, Y.-C.; Hsu, C.-W.; Yu, J.-S. K.; Lee, G.-H.; Wang, Y.; Kuo, T.-S. *Angew. Chem. Int. Ed.* **2008**, *47* (38), 7250. doi:10.1002/anie.200801286.; (d) Horvath, S.; Gorelsky, S. I.; Gambarotta, S.; Korobkov, I. *Angew. Chem. Int. Ed.* **2008**, *47* (51), 9937. doi:10.1002/anie.200804048.

(7) (a) Kurokawa, Y. I.; Nakao, Y.; Sakaki, S. *J. Phys. Chem. A* **2009**, *113* (13), 3202. doi:10.1021/jp809597m. PMID:19271722.; (b) Saito, K.; Nakao, Y.; Sato, H.; Sakaki, S. *J. Phys. Chem. A* **2006**, *110* (31), 9710. doi:10.1021/jp057558j. PMID:16884203.

(8) Braunstein, P.; Rose, J. In *Comprehensive Organometallic Chemistry II: A Review of the Literature 1982–1994;* Abel,

E. W., Stone, F. G. A., Wilkinson, G., Eds.; Pergamon: New York, 1995; Vol. 10.
(9) Chetcuti, M. J. In *Comprehensive Organometallic Chemistry II: A Review of the Literature 1982–1994;* Abel, E. W., Stone, F. G. A., Wilkinson, G., Eds.; Pergamon: New York, 1995; Vol. 10.
(10) Gade, L. H. *Angew. Chem.* **2000**, *112* (15), 2768. doi:10.1002/1521-3757(20000804)112:15<2768::AID-ANGE2768>3.0.CO;2-0.
(11) Wheatley, N.; Kalck, P. *Chem. Rev.* **1999**, *99* (12), 3379. doi:10.1021/cr980325m. PMID:11849025.
(12) Collman, J. P.; Boulatov, R. *Angew. Chem.* **2002**, *114* (21), 4120. doi:10.1002/1521-3757(20021104)114:21<4120::AID-ANGE4120>3.0.CO;2-N.
(13) Slater, J. C. *Quantum Theory of Molecules and Solids;* McGraw-Hill: New York, 1974; Vol. 4.
(14) Vosko, S. H.; Wilk, L.; Nusair, M. *Can. J. Phys.* **1980**, *58* (8), 1200. doi:10.1139/p80-159.
(15) Becke, A. D. *Phys. Rev. A* **1988**, *38* (6), 3098. doi:10.1103/PhysRevA.38.3098. PMID:9900728.
(16) Perdew, J. P. *Phys. Rev. B* **1986**, *33* (12), 8822. doi:10.1103/PhysRevB.33.8822.
(17) Lee, C.; Yang, W.; Parr, R. G. *Phys. Rev. B* **1988**, *37* (2), 785. doi:10.1103/PhysRevB.37.785.
(18) Handy, N. C.; Cohen, A. J. *Mol. Phys.* **2001**, *99* (5), 403. doi:10.1080/00268970010018431.
(19) Perdew, J. P.; Burke, K.; Ernzerhof, M. *Phys. Rev. Lett.* **1996**, *77* (18), 3865. doi:10.1103/PhysRevLett.77.3865. PMID:10062328.
(20) Hamprecht, F. A.; Cohen, A. J.; Tozer, D. J.; Handy, N. C. *J. Chem. Phys.* **1998**, *109* (15), 6264. doi:10.1063/1.477267.
(21) Stephens, P. J.; Devlin, F. J.; Chabalowski, C. F.; Frisch, M. J. *J. Phys. Chem.* **1994**, *98* (45), 11623. doi:10.1021/j100096a001.
(22) Frisch, M. J.; Trucks, G. W.; Schlegel, H. B.; Scuseria, G. E.; Robb, M. A.; Cheeseman, J. R.; Montgomery, J. A., Jr.; Vreven, T.; Kudin, K. N.; Burant, J. C.; Millam, J. M.; Iyengar, S. S.; Tomasi, J.; Barone, V.; Mennucci, B.; Cossi, M.; Scalmani, G.; Rega, N.; Petersson, G. A.; Nakatsuji, H.; Hada, M.; Ehara, M.; Toyota, K.; Fukuda, R.; Hasegawa, J.; Ishida, M.; Nakajima, T.; Honda, Y.; Kitao, O.; Nakai, H.; Klene, M.; Li, X.; Knox, J. E.; Hratchian, H. P.; Cross, J. B.; Bakken, V.; Adamo, C.; Jaramillo, J.; Gomperts, R.; Stratmann, R. E.; Yazyev, O.; Austin, A. J.; Cammi, R.; Pomelli, C.; Ochterski, J. W.; Ayala, P. Y.; Morokuma, K.; Voth, G. A.; Salvador, P.; Dannenberg, J. J.; Zakrzewski, V. G.; Dapprich, S.; Daniels, A. D.; Strain, M. C.; Farkas, O.; Malick, D. K.; Rabuck, A. D.; Raghavachari, K.; Foresman, J. B.; Ortiz, J. V.; Cui, Q.; Baboul, A. G.; Clifford, S.; Cioslowski, J.; Stefanov, B. B.; Liu, G.; Liashenko, A.; Piskorz, P.; Komaromi, I.; Martin, R. L.; Fox, D. J.; Keith, T.; Al-Laham, M. A.; Peng, C. Y.; Nanayakkara, A.; Challacombe, M.; Gill, P. M. W.; Johnson, B.; Chen, W.; Wong, M. W.; Gonzalez, C.; Pople, J. A. *Gaussian03,* revision D01; Gaussian, Inc.: Wallingford, CT, 2004.
(23) Hoe, W.-M.; Cohen, A. J.; Handy, N. C. *Chem. Phys. Lett.* **2001**, *341* (3–4), 319. doi:10.1016/S0009-2614(01)00581-4.
(24) Xu, X.; Goddard, W. A., III. *Proc. Natl. Acad. Sci. U.S.A.* **2004**, *101* (9), 2673. doi:10.1073/pnas.0308730100. PMID:14981235.
(25) Tao, J.; Perdew, J. P.; Staroverov, V. N.; Scuseria, G. E. *Phys. Rev. Lett.* **2003**, *91* (14), 146401. doi:10.1103/PhysRevLett.91.146401. PMID:14611541.
(26) Van Voorhis, T.; Scuseria, G. E. *J. Chem. Phys.* **1998**, *109* (2), 400. doi:10.1063/1.476577.
(27) Weigend, F. *Phys. Chem. Chem. Phys.* **2006**, *8* (9), 1057. doi:10.1039/b515623h. PMID:16633586.
(28) Weigend, F.; Ahlrichs, R. *Phys. Chem. Chem. Phys.* **2005**, *7* (18), 3297. doi:10.1039/b508541a. PMID:16240044.
(29) Andrae, D.; Häußermann, U.; Dolg, M.; Stoll, H.; Preuß, H. *Theor. Chim. Acta* **1990**, *77* (2), 123. doi:10.1007/BF01114537.
(30) Čížek, J. *J. Chem. Phys.* **1966**, *45* (11), 4256. doi:10.1063/1.1727484.
(31) Bartlett, R. J.; Purvis, G. D. *Int. J. Quantum Chem.* **1978**, *14* (5), 561. doi:10.1002/qua.560140504.
(32) Hampel, C.; Peterson, K.; Werner, H.-J. *Chem. Phys. Lett.* **1992**, *190* (1–2), 1. doi:10.1016/0009-2614(92)86093-W.
(33) Pople, J. A.; Head-Gordon, M.; Raghavachari, K. *J. Chem. Phys.* **1987**, *87* (10), 5968. doi:10.1063/1.453520.
(34) Pople, J. A.; Krishnan, R.; Schlegel, H. B.; Binkley, J. S. *Int. J. Quantum Chem.* **1978**, *14* (5), 545. doi:10.1002/qua.560140503.
(35) Purvis, G. D.; Bartlett, R. J. *J. Chem. Phys.* **1982**, *76* (4), 1910. doi:10.1063/1.443164.
(36) Werner, H.-J.; Knowles, P. J.; Lindh, R.; Manby, F. R.; Schütz, M.; Celani, P.; Korona, T.; Rauhut, G.; Amos, R. D.; Bernhardsson, A.; Berning, A.; Cooper, D. L.; Deegan, M. J. O.; Dobbyn, A. J.; Eckert, F.; Hampel, C.; Hertzer, G.; Lloyd, A. W.; McNicholas, S. J.; Meyer, W.; Mura, M. E.; Nicklass, A.; Palmieri, P.; Pitzer, R.; Schumann, U.; Stoll, H.; Stone, A. J.; Tarroni, R.; Thorsteinsson, T. *MOLPRO,* version 2006.1; a package of ab initio programs; 2006. Available from http://www.molpro.net.
(37) Roos, B. O. In *Advances in Chemical Physics: Ab initio Methods in Quantum Chemistry;* Lawley, K. P., Ed.; John Wiley & Sons Ltd.: Chichester, UK, 1987; Vol. II, p 399.
(38) Andersson, K.; Malmqvist, P.-Å.; Roos, B. O.; Sadlej, A. J.; Wolinski, K. *J. Phys. Chem.* **1990**, *94* (14), 5483. doi:10.1021/j100377a012.
(39) Andersson, K.; Malmqvist, P.-Å.; Roos, B. O. *J. Chem. Phys.* **1992**, *96* (2), 1218. doi:10.1063/1.462209.
(40) Roos, B. O.; Andersson, K.; Fülscher, M. P.; Malmqvist, P.-Å.; Serrano-Andrés, L.; Pierloot, K.; Merchán, M. In *Advances in Chemical Physics: New Methods in Computational Quantum Mechanics;* Prigogine, I., Rice, S. A., Eds.; John Wiley & Sons Ltd.: Chichester, UK, 1996; Vol. XCIII; p 219.
(41) Douglas, N.; Kroll, N. M. *Ann. Phys.* **1974**, *82* (1), 89. doi:10.1016/0003-4916(74)90333-9.
(42) Hess, B. *Phys. Rev. A* **1986**, *33* (6), 3742. doi:10.1103/PhysRevA.33.3742.
(43) Karlström, G.; Lindh, R.; Malmqvist, P.-Å.; Roos, B. O.; Ryde, U.; Veryazov, V.; Widmark, P.-O.; Cossi, M.; Schimmelpfennig, B.; Neogrady, P.; Seijo, L. *Comput. Mater. Sci.* **2003**, *28* (2), 222. doi:10.1016/S0927-0256(03)00109-5.
(44) Reed, A. E.; Curtiss, L. A.; Weinhold, F. *Chem. Rev.* **1988**, *88* (6), 899. doi:10.1021/cr00088a005.
(45) Morokuma, K. *J. Chem. Phys.* **1971**, *55* (3), 1236. doi:10.1063/1.1676210.
(46) Kitaura, K.; Morokuma, K. *Int. J. Quantum Chem.* **1976**, *10* (2), 325. doi:10.1002/qua.560100211.
(47) Bickelhaupt, F. M.; Baerends, E. J. In *Reviews in Computational Chemistry;* Lipkowitz, K. B., Boyd, D. B., Eds.; Wiley-VCH: New York, 2000; Vol. 15, p 1.
(48) Ziegler, T.; Rauk, A. *Theor. Chim. Acta* **1977**, *46* (1), 1. doi:10.1007/BF02401406.

(49) Ziegler, T.; Rauk, A. *Inorg. Chem.* **1979**, *18* (7), 1755. doi:10.1021/ic50197a006.
(50) Snijders, J. G.; Baerends, E. J.; Vernooijs, P. *At. Data Nucl. Data Tables (N.Y.)* **1981**, *26* (6), 483. doi:10.1016/0092-640X(81)90004-8.
(51) Chang, C.; Pelissier, M.; Durand, P. *Phys. Scr.* **1986**, *34* (5), 394. doi:10.1088/0031-8949/34/5/007.
(52) Heully, J.-L.; Lindgren, I.; Lindroth, E.; Lundqvist, S.; Martensson-Pendrill, A.-M. *J. Phys. B* **1986**, *19* (18), 2799. doi:10.1088/0022-3700/19/18/011.
(53) van Lenthe, E.; Baerends, E. J.; Snijders, J. G. *J. Chem. Phys.* **1993**, *99* (6), 4597. doi:10.1063/1.466059.
(54) van Lenthe, E.; van Leeuwen, R.; Baerends, E. J.; Snijders, J. G. *Int. J. Quantum Chem.* **1996**, *57* (3), 281. doi:10.1002/(SICI)1097-461X(1996)57:3<281::AID-QUA2>3.0.CO;2-U.
(55) van Lenthe, E.; Snijders, J. G.; Baerends, E. J. *J. Chem. Phys.* **1996**, *105* (15), 6505. doi:10.1063/1.472460.
(56) te Velde, G.; Bickelhaupt, F. M.; Baerends, E. J.; Van Fonseca Guerra, C.; van Gisbergen, S. J. A.; Snijders, J. G.; Ziegler, T. *J. Comput. Chem.* **2001**, *22* (9), 931. doi:10.1002/jcc.1056.
(57) Scientific Computing & Modelling (SCM). *ADF2005.01*; SCM, Theoretical Chemistry, Vrije Universiteit: Amsterdam, The Netherlands. Available from http://www.scm.com.
(58) Cavigliasso, G.; Kaltsoyannis, N. *Dalton Trans.* **2006**, 5476. doi:10.1039/b613446g. PMID:17117217.
(59) Cotton, F. A.; Daniels, L.; Davison, A.; Orvig, C. *Inorg. Chem.* **1981**, *20* (9), 3051. doi:10.1021/ic50223a058.
(60) Poineau, F.; Sattelberger, A. P.; Conradson, S. D.; Czerwinski, K. R. *Inorg. Chem.* **2008**, *47* (6), 1991. doi:10.1021/ic701453k. PMID:18290609.
(61) Cramer, C. J.; Truhlar, D. G. *Phys. Chem. Chem. Phys.* **2009**, *11* (46), 10757. doi:10.1039/b907148b. PMID:19924312.
(62) Zhao, Y.; Schultz, N. E.; Truhlar, D. G. *J. Chem. Theory Comput.* **2006**, *2* (2), 364. doi:10.1021/ct0502763.
(63) Cotton, F. A.; Murillo, C. A.; Walton, R. A. *Multiple Bonds Between Metal Atoms,* 3rd ed.; Springer Science and Business Media, Inc.: New York, 2005; p 724.
(64) Furche, F.; Perdew, J. P. *J. Chem. Phys.* **2006**, *124* (4), 044103. doi:10.1063/1.2162161. PMID:16460145.
(65) Schultz, N. E.; Zhao, Y.; Truhlar, D. G. *J. Phys. Chem. A* **2005**, *109* (19), 4388. doi:10.1021/jp0504468. PMID:16833770.
(66) Gagliardi, L.; Roos, B. O. *Inorg. Chem.* **2003**, *42* (5), 1599. doi:10.1021/ic0261068. PMID:12611528.
(67) Saito, K.; Nakao, Y.; Sato, H.; Sakaki, S. *J. Phys. Chem. A* **2006**, *110* (31), 9710. doi:10.1021/jp057558j. PMID:16884203.
(68) All orbital contributions presented in this section are based on the MO coefficients at the BP86/TZ2P level.
(69) This result has been discussed in detail in Krapp, A.; Lein, M.; Frenking, G. *Theor. Chem. Acc.* **2008**, *120* (1–3), 313. doi:10.1007/s00214-007-0294-6.
(70) (a) Diefenbach, A.; Bickelhaupt, F. M.; Frenking, G. *J. Am. Chem. Soc.* **2000**, *122* (27), 6449. doi:10.1021/ja000663g.; (b) Boehme, C.; Uddin, J.; Frenking, G. *Coord. Chem. Rev.* **2000**, *197* (1), 249. doi:10.1016/S0010-8545(99)00227-1.; (c) Uddin, J.; Frenking, G. *J. Am. Chem. Soc.* **2001**, *123* (8), 1683. doi:10.1021/ja002845g. PMID:11456768.
(71) Spackman, M. A.; Maslen, E. N. *J. Phys. Chem.* **1986**, *90* (10), 2020. doi:10.1021/j100401a010.
(72) (a) Krapp, A.; Bickelhaupt, F. M.; Frenking, G. *Chem. Eur. J.* **2006**, *12* (36), 9196. doi:10.1002/chem.200600564.; (b) Kovács, A.; Esterhuysen, C.; Frenking, G. *Chem. Eur. J.* **2005**, *11* (6), 1813 doi:10.1002/chem.200400525.; (c) Esterhuysen, C.; Frenking, G. *Theor. Chem. Acc.* **2004**, *111* (2–6), 381. doi:10.1007/s00214-003-0535-2.
(73) Frenking, G.; Fröhlich, N. *Chem. Rev.* **2000**, *100* (2), 717. doi:10.1021/cr9804011.